

**Universal scaling of charge-order melting in the magnetic field–pressure–temperature landscape**Sudip Pal, Kranti Kumar, and A. Banerjee *UGC DAE Consortium for Scientific Research, Khandwa Road, University Campus, Indore-452001, India*

(Received 11 August 2020; accepted 26 October 2020; published 11 November 2020)

We show that the first-order transition related to charge ordering (CO) follows power-law scaling with external hydrostatic pressure ( $P$ ) and magnetic field ( $H$ ). This is an experimental evidence of a scaling relation through magnetization measurement across the CO transition temperature ( $T_{\text{CO}}$ ) in three manganese-oxide systems under the simultaneous influence of  $H$  and  $P$ . The melting of CO instability obeys a simple scaling relation,  $\Delta T_{\text{CO}} = f(HP^\alpha)$ , where  $\Delta T_{\text{CO}}$  is the suppression of  $T_{\text{CO}}$  by  $P$  and  $H$  and  $\alpha$  is the nonuniversal scaling exponent that crucially depends on lattice, charge, and spin coupled dynamics. Our results suggest that the instability point of a first-order transition scales with the strength of the perturbations,  $H$  and  $P$ . The  $H$ - $P$ - $T$  scaling should allow us controlled manipulation of the transition in a three-dimensional space. The scaling relations should be applicable to other first-order transitions as well with the relevant parameters.

DOI: [10.1103/PhysRevB.102.201109](https://doi.org/10.1103/PhysRevB.102.201109)

Critical phenomena is an interesting subject and is spread over diverse disciplines. The scaling relations among relevant parameters nicely describe the chaotic dynamics of the continuous phase transitions and various other disparate events such as in neural networks, avalanches in sandpiles, earthquakes, fluctuations in the stock market, etc. [1,2]. First-order transitions also show critical slowing down while approaching spinodal temperatures, which are the limits of the metastability [3,4]. This phenomenon is controlled by “critical-like singularity” [5–7]. In the mean-field approximation, the correlation length and the relaxation time should diverge at the spinodal. Nonetheless, despite its prevalence in various branches of science, the understanding of first-order transitions remained at a nascent stage. It is yet to develop in terms of the scaling and its universality. In real finite-dimensional systems the thermal fluctuations smear the mean-field spinodals if the fluctuations are comparable to the nucleation barrier. There one can still assume a hidden spinodal, which is called an “instability point,” and the associated scaling should remain intact [8,9].

The critical phenomena across first-order phase transition remained mostly unattended until recently after it has been experimentally observed across the charge-order (CO) transition, Mott transition, and nematic-smectic phase transitions [10–13]. The dynamics of a first-order transition is controlled by the unstable fixed point and it obeys scaling laws with unstable exponents contrary to the stable fixed point in the case of continuous transitions [8,14]. In the case of a temperature driven first-order transition, the transition temperature obeys power-law scaling with the temperature sweep rate ( $R$ ) [8–14]. In addition, in the case of magnetic transitions, it should be dependent on  $H$  also, which is evident from the equation of state of the first-order transition [8]. In this context, we have studied the shift of the CO transition temperature ( $T_{\text{CO}}$ ) with the strength of the magnetic field ( $H$ ) and pressure ( $P$ ). From the experimental data, we demonstrate the power-law

scaling between  $T_{\text{CO}}$  and  $H$ . We further show the universal scaling of  $T_{\text{CO}}$ ,  $P$ , and  $H$  described by a nonuniversal scaling exponent. This is an experimental evidence of scaling in a three-dimensional space including pressure, magnetic field, and temperature across the first-order transition.

The CO state appears in mixed valence systems having a narrow electron bandwidth where below the CO transition temperature ( $T_{\text{CO}}$ ) the charges form a spatially ordered ground state [15]. Examples of the prominent CO system include a variety of oxides, organic compounds, high- $T_{\text{C}}$  superconductors, etc. [16–24]. The intriguing interplay of structural parameters, spins, and charges in the CO transition is exceedingly mysterious and yet an utterly unsolved problem [19–22]. Signatures of critical behavior across the transition have been observed in neutron- and light-scattering measurements [23,24]. In our study,  $T_{\text{CO}}$  decreases with increasing  $H$  and  $P$ . The effect of  $H$  is nonlinear and is progressively pronounced at higher  $P$ . Whereas, the effect of  $P$  is linear and progressively increases at higher  $H$ . The main result of our work is that the suppression of  $T_{\text{CO}}$  obeys power-law scaling with the strength of the perturbation, which is  $H$  in our case. We propose an intriguing role of  $P$  in this context. In addition,  $T_{\text{CO}}$ ,  $P$ , and  $H$  can be scaled onto a single master curve by a simple empirical scaling relation,  $\Delta T_{\text{CO}} = f(HP^\alpha)$ . Here,  $\Delta T_{\text{CO}}$  is the change in  $T_{\text{CO}}$  by  $H$  at pressure  $P$  and  $\alpha$  is a scaling constant, which is the only free parameter here. The scaling behavior is an indication of the evolution of the CO state in a self-similar way under  $P$  and  $H$ . We explain it as the manifestation of spinodal singularity related to the CO transition and the coefficient  $\alpha$  is a nonuniversal exponent that is decided by the complicated coupling among the spin charge and lattice degrees of freedom.

We have studied three CO systems:  $\text{Pr}_{0.5}\text{Ca}_{0.5}\text{MnO}_3$  (PCMO1),  $\text{Pr}_{0.5}\text{Ca}_{0.5}\text{Mn}_{0.975}\text{Al}_{0.025}\text{O}_3$  (PCMAO), and  $\text{Pr}_{0.6}\text{Ca}_{0.4}\text{MnO}_3$  (PCMO2). The CO transitions in these systems show a prominent peak at the transition temperature

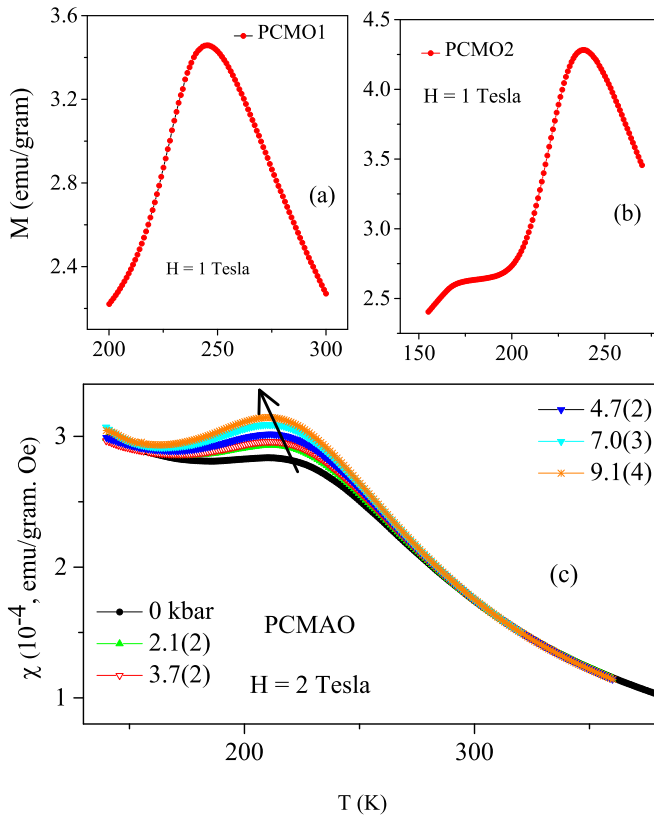


FIG. 1. (a) and (b) show the  $M$ - $T$  curve of PCMO1 and PCMO2 around CO transition. It shows a prominent peak at  $T_{CO}$ . The measurement field is  $H = 1$  tesla. PCMO2 shows antiferromagnetic transition around 170 K. (c) it is the temperature variation of susceptibility of PCMAO at a constant measuring field of  $H = 2$  tesla. We have also shown the effect of  $P$ . The uncertainty in the last digit of  $P$  values is shown in parentheses.

and thermal hysteresis in the  $M$ -temperature ( $T$ ) measurement which is reminiscent of the first-order transition. The spin, lattice, and charge dynamics are strongly interwoven, which is evident in the recent experimental observations of novel phenomena such as lattice driven magnetic order, metal-insulator transition, etc. [19–21]. PCMO1 is a very robust CO system and PCMAO and PCMO2 provide two different pathways to study a weaker CO state under  $P$  and  $H$ . In PCMAO, 2.5% Al doping breaks the long-range CO correlation present in PCMO1, whereas PCMO2 has dominating ferromagnetic (FM) correlation. Depending on  $x$ ,  $\text{Pr}_{1-x}\text{Ca}_x\text{MnO}_3$  undergoes a transition into a charge/orbital ordered state below 220–245 K, subsequently followed by an antiferromagnetic phase at around 140–170 K [25].

The polycrystalline samples are prepared by standard solid-state reaction and characterized by x-ray diffraction and iodometric titration [26]. The details of the sample preparation and characterization can be found in Ref. [26]. The CO and antiferromagnetic transition temperatures match with the earlier reports which further confirm the integrity of the samples. However, PCMO2 has been found to show a spurious peak in the  $M$ - $T$  below  $T_{CO}$  only above 5 tesla at ambient pressure, although laboratory based x-ray diffraction does not reveal the presence of any impurity. Therefore, for this compound we

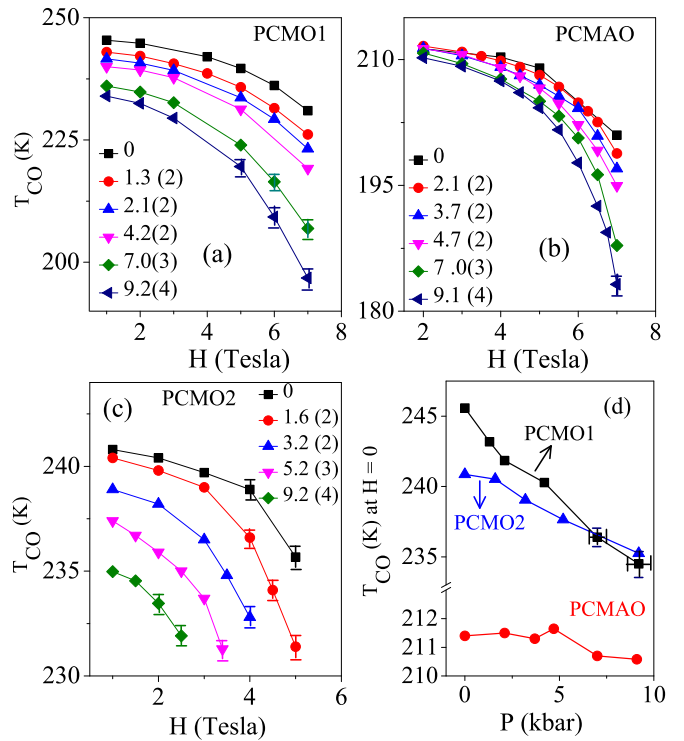


FIG. 2. (a)–(c) Shift of  $T_{CO}$  as a function of  $H$  in PCMO1, PCMAO, and PCMO2, respectively. Different curves represent different  $P$  values. (d) The variation of  $T_0$  with  $P$ .  $T_0$  values have been obtained by following Eq. (1). Solid lines are a guide for the eyes. The uncertainty in the last digit of the  $P$  values is mentioned in parentheses.

have reported the  $T_{CO}$  values in a limited  $H$ - $P$  region where its value can be obtained unambiguously.  $M$ - $T$  measurements are performed in a 7 tesla SQUID magnetometer (M/S Quantum Design, USA). For external hydrostatic pressure, a Cu-Be pressure cell with pressure limit of 10 kbar (easyLabMcell 10) has been used. Daphne oil has been used as a pressure transmitting medium. Reported  $P$  values are determined by monitoring the superconducting transition temperature of Sn loaded inside the pressure cell [27].

At room temperature PCMO1, PCMAO, and PCMO2 samples are paramagnetic insulators. On cooling from the paramagnetic state, they show a prominent peak in magnetization ( $T$ ) around  $T_{CO} = 245$ , 211.5, and 240 K, respectively, as shown in Figs. 1(a)–1(c). An additional feature corresponding to antiferromagnetic transition is clearly observed in PCMO2 around  $T = 170$  K. In Fig. 1(c), we also show the representative data showing the effect of  $P$  on PCMAO for the applied magnetic field of  $H = 2$  tesla. All the measurements have been performed in the cooling cycle. External  $P$  destabilizes the CO state and drives  $T_{CO}$  progressively toward lower temperature. Note that, at high  $T$  all susceptibility,  $\chi$  ( $= M/H$ , where  $M$  is the dc magnetization) curves at different  $P$  are merged but as temperature is reduced toward  $T_{CO}$ , they start deviating from each other. The deviation is more pronounced just above  $T_{CO}$ . We have taken the temperature where susceptibility is maximum as  $T_{CO}$ . In Figs. 2(a)–2(c), we show the variation of  $T_{CO}$  with  $P$  and  $H$  for PCMO1, PCMAO, and PCMO2, respectively [28]. In all three systems, suppression

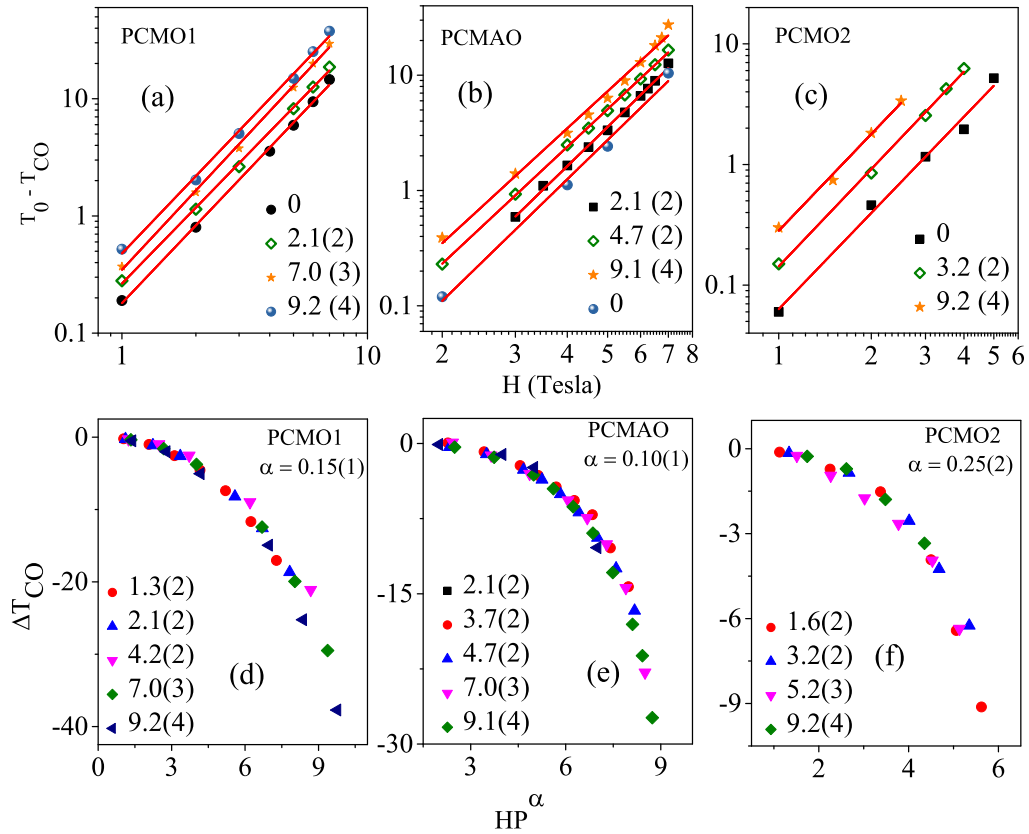


FIG. 3. (a)–(c) Double logarithmic plot of  $T_0 - T_{CO}$  and  $H$  for PCMO1, PCMAO, and PCMO2 following Eq. (1). Red solid lines are fitted straight lines. Data of a few  $P$  values have been shown to maintain clarity. (d)–(f) Scaling of  $T_{CO}$ ,  $P$ , and  $H$  for the three samples following Eq. (2). Legends indicate the  $P$  values in the unit of kbar. The uncertainty in the last digit of the  $P$  values is mentioned in parentheses.

of the transition temperature by  $H$  is nonlinear and more rapid at higher  $P$ . The uncertainties in  $T_{CO}$  are smaller than the width of the symbols unless mentioned in the figure.

In the case of a temperature driven first-order transition, the transition temperature obeys a scaling relation with the temperature sweep rate ( $R$ ), which is given by  $A_t = A_0 + aR^\gamma$ , where  $\gamma$  is the critical exponent and “ $a$ ” is a constant [10,14]. Here, to analyze the effect of  $H$ , we use similar power-law dependence, given by

$$T_{CO} = T_0 + a(P)H^\gamma, \quad (1)$$

where  $T_0$  is the  $T_{CO}$  at  $H = 0$  and as we will show the coefficient “ $a$ ” is dependent on  $P$ . We have shown the power-law dependence of  $T_{CO}$  in Figs. 3(a)–3(c). We have chosen the  $T_0$  value that gives the best straight line and the variation is shown in Fig. 2(d). The interesting point to note here is that  $P$  does not affect the slope of the curves, which means  $P$  does not significantly change the exponent  $\gamma$  as shown in Fig. 4, rather it only affects the coefficient “ $a$ ” (intercept in the log-log plot). In fact,  $\log a(P)$  is nearly a linear function of  $P$  as evident from Figs. 3(a)–3(c); however, to find the exact functional form, more close data points are necessary. The linear dependence of the intercept on  $P$  is indeed interesting. Because, following Eq. (1), it can be proved that the linear dependence of the intercept on  $P$  indicates the exponential dependence of the coefficient “ $a$ ” on  $P$ . At low  $P$  values,  $T_{CO}$  will vary linearly with  $P$ ; however, at higher  $P$  there will be a crossover to nonlinear effects in the presence of  $H$ .

The  $T_{CO} - T_0 = \Delta T_{CO}$  (say) at different  $P$  underline the effect of  $H$  on  $T_{CO}$  at respective  $P$  values. In Figs. 3(d)–3(f), we have plotted  $\Delta T_{CO}$  as the y axis and a scaled x axis as  $HP^\alpha$ , for the three systems, where  $\alpha$  is a constant. It shows that all data points collapse onto a single master curve. This curve also merges with the  $\Delta T_{CO}$  vs  $H$  data measured at ambient  $P$  (not shown here for clarity). Such data collapse implies that the melting of the CO state under the simultaneous action of  $P$  and  $H$  obeys a single scaling relation:

$$\Delta T_{CO} = f(HP^\alpha), \quad (2)$$

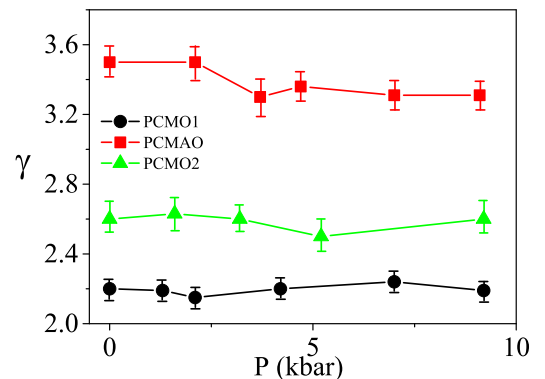


FIG. 4. Variation of  $\gamma$  with  $P$  obtained from the straight line fit in Figs. 3(a)–3(c).

where  $f$  denotes an arbitrary function. The obtained values of  $\alpha$  for PCMO1, PCMAO, and PCMO2 are 0.15, 0.10, and 0.25, respectively. The functional dependence between  $\Delta T_{\text{CO}}$  and  $P, H$  in Eq. (2) is the natural guess for us because the  $T_{\text{CO}}$  is suppressed by both  $H$  and  $P$  and the effect of  $H$  is progressively enhanced at higher pressure. It may be noted here that the data collapse can also be obtained by using the more conventional functional relations, for example  $\Delta T_{\text{CO}}/P^\beta = f(HP^\alpha)$ , but we have not taken this equation forward because of the possible ambiguity in varying two adjustable parameters,  $\alpha$  and  $\beta$ .

$\text{Pr}_{1-x}\text{Ca}_x\text{MnO}_3$  crystallizes in the orthorhombically distorted structure. The structural distortion largely occurs due to a variation in the  $\text{Mn}^{3+}/\text{Mn}^{4+}$  concentration having different ionic radius and the cooperative Jahn-Teller (JT) distortion of  $\text{Mn}^{3+}$ . The CO state is very robust in  $\text{Pr}_{0.5}\text{Ca}_{0.5}\text{MnO}_3$  and relatively weaker for  $x < 0.5$  due to dominating ferromagnetic interaction. External  $H$  reduces spin disorder and enhances the FM correlation. It increases the conduction bandwidth of  $e_g$  orbital electrons in  $\text{Mn}^{3+}$  and thereby weakens the CO state as observed in Figs. 2(a)–2(c). In addition,  $H$  reduces the JT distortion as well [29]. On the other hand, external  $P$  compresses the volume, so that it straightens the Mn-O-Mn angle and reduces the Mn-O bond length [15]. This results in an increase in bare transfer integral ( $t_0$ ) of the system and delocalizes the charge carriers [15]. Therefore,  $P$  reduces  $T_{\text{CO}}$  and melts the CO-insulating state into a conducting state. It also promotes the FM correlation due to an enhanced double exchange (DE) interaction. Apart from  $t_0$ ,  $P$  is also expected to reduce the dynamical electron-phonon coupling [30,31] that tends to localize the charge carriers by forming JT polarons, a coupled electron-lattice entity. Overall,  $P$  raises the effective transfer integral ( $t_{\text{eff}}$ ) of  $e_g$  orbital electrons, resulting in a continuous abatement of electron-lattice coupling. A scaling relation further indicates that the modifications of lattice and spin by  $P, H$  and finally their effects on charge dynamics are not arbitrary, but rather nicely intertwined. In our scaling relation, the exponent  $\alpha$  appears to be nonuniversal.

The universality or the nonuniversality of a scaling relation to date is least understood in the case of a critical phenomenon [32–34]. Chemical substitution, short-range interaction, and JT distortion deviates a system from a pure universality class [35,36]. The interplay between different intrinsic parameters such as structural distortion and spin-spin correlation significantly affect the critical behavior in high- $T_c$  superconductors, Mott transition, metal-insulator transitions, etc. [37–39]. The first-order transitions in magnetic systems frequently accompany strong and abrupt structural distortions together with modifications in charge and orbital dynamics, and hence can be controlled by  $P$  and  $H$ . In the following, we will discuss how such coupling might be significant in the case of CO transition as observed in our scaling relation.

In Fig. 2(d), we have compared the drop in  $T_{\text{CO}}$  by  $P$  at  $H = 0$  for the three systems. If we compare PCMO1 and PCMO2,  $P$  suppressed  $T_{\text{CO}}$  by a larger extent in PCMO1 than

in PCMO2. This can be understood from the fact that PCMO2 contains a higher fraction of  $\text{Mn}^{3+}$ , and therefore it has larger JT distortion as compared to PCMO1. It is expected to give rise to a stronger electron-lattice coupling in PCMO2 [30] and therefore requires larger pressure to melt the CO state. On the contrary, the effect of magnetic field on  $T_{\text{CO}}$  is more prominent in PCMO2, which is reflected by the higher value of  $\gamma$  shown in Fig. 4. This is because PCMO2 is more prone to the FM state due to a dominant FM interaction. As a result, magnetic field suppresses the CO state more strongly in PCMO2 than in PCMO1.

On the other hand, in PCMAO, where 2.5% Al is substituted in PCMO1,  $\text{Al}^{3+}$  replaces the  $\text{Mn}^{4+}$  and does not significantly alter the crystal structure [26]. However, random substitution of Mn ions by nonmagnetic element Al breaks the long-range  $\text{Mn}^{3+}\text{-O-Mn}^{4+}$  chains in PCMO1 into finite segments and weakens the CO state. This explains the observation that in PCMAO, the effect of  $P$  on  $T_{\text{CO}}$  at  $H = 0$  (i.e.,  $T_0$ ) is insignificant compared to the parent compound PCMO1 [see Fig. 2(d)]. It indicates that the impact of  $P$  on a system crucially depends on the underlying length scale. Note that the effect of  $H$  on  $T_{\text{CO}}$  is large, which is possibly due to a weak CO state. On the other hand, transport measurements show that polaron hopping energy decreases by Al substitution, which is due to an increase in  $\text{Mn}^{4+}$  to meet charge neutrality [26]. This should result in reduced JT distortion that may not be visible in laboratory x-ray diffraction measurements. Overall, the value of  $\gamma$  is highest for PCMAO. Therefore, the effect of  $H$  and  $P$  on these systems crucially depends on their underlying spin, lattice, and charge degrees of freedom. We strongly believe that the interplay of these things crucially affects the power-law scaling between  $T_{\text{CO}}$  and  $H$  and finally the scaling relation between  $T_{\text{CO}}, P$ , and  $H$  as shown in Fig. 3.

In brief, we have studied the suppression of the CO state by  $P$  and  $H$  through magnetization measurements in three manganite systems. This is a first-order transition. The melting process in the  $H$ - $P$ - $T$  landscape is not arbitrary and follows scaling relations which should be applicable for other first-order transitions. In addition, the understanding of the first-order transition and the CO state is recently going through a revolutionary change, therefore the observed scaling behavior in the melting process and its direct connection with electron, spin, and lattice coupling should be useful to further elucidate these phenomena. Simultaneously, the present study calls for serious scrutiny of the CO state in other systems and instigates bringing in other relevant parameters such as electric field. The scaling of transition temperature will enable us controlled utilization of different parameters to manipulate a transition which is a cornerstone of contemporary research. We further believe that the inclusion of  $P$  as a scaling variable in other kinds of phase transitions, which is rare at this time, would be interesting and informative.

We gratefully acknowledge Dr. S. B. Roy and Dr. Fan Zhong for important discussions.

[1] H. E. Stanley, *Introduction to Phase Transition and Critical Phenomena* (Oxford University Press, New York, 1984).

[2] J. P. Sethna, K. A. Dahmen, and C. R. Myers, *Nature (London)* **410**, 242 (2001).

- [3] M. E. Fisher and A. N. Berker, *Phys. Rev. B* **26**, 2507 (1982).
- [4] A. Compagner, *Physica* **72**, 115 (1974).
- [5] K. Binder, *Rep. Prog. Phys.* **50**, 783 (1987).
- [6] X. An, D. Mesterházy, and M. A. Stephanov, *J. Stat. Mech.* (2018) 033207.
- [7] C. Sasaki, B. Friman, and K. Redlich, *Phys. Rev. Lett.* **99**, 232301 (2007).
- [8] N. Liang and F. Zhong, *Front. Phys.* **12**, 126403 (2017).
- [9] Fan Zhong, *J. Phys.: Condens. Matter* **30**, 445401 (2018).
- [10] T. Bar, S. K. Choudhary, Md. A. Ashraf, K. S. Sujith, S. Puri, S. Raj, and B. Bansal, *Phys. Rev. Lett.* **121**, 045701 (2018).
- [11] S. Kundu, T. Bar, R. K. Nayak, and B. Bansal, *Phys. Rev. Lett.* **124**, 095703 (2020).
- [12] Y. Zhu, J. Hoffman, C. E. Rowland, H. Park, D. A. Walko, J. W. Freeland, P. J. Ryan, R. D. Schaller, A. Bhattacharya, and H. Wen, *Nat. Commun.* **9**, 1799 (2018).
- [13] T. Furukawa, K. Kobashi, Y. Kurosaki, K. Miyagawa, and K. Kanoda, *Nat. Commun.* **9**, 307 (2018).
- [14] Fan Zhong and Qizhou Chen, *Phys. Rev. Lett.* **95**, 175701 (2005).
- [15] Y. Moritomo, H. Kuwahara, Y. Tomioka, and Y. Tokura, *Phys. Rev. B* **55**, 7549 (1997).
- [16] P. Adler, P. Jeglič, M. Reehuis, M. Geiß, P. Merz, T. Knaflič, M. Komelj, A. Hoser, A. Sans, J. Janek, D. Arčon, M. Jansen, and C. Felser, *Sci. Adv.* **4**, eaap7581 (2018).
- [17] A. Pustogow, Y. Saito, A. Rohwer, J. A. Schlueter, and M. Dressel, *Phys. Rev. B* **99**, 140509(R) (2019).
- [18] E. H. da Silva Neto, R. Comin, F. He, R. Sutarto, Y. Jiang, R. L. Greene, G. A. Sawatzky, and A. Damascelli, *Science* **347**, 282 (2015).
- [19] V. Esposito *et al.*, *Phys. Rev. Lett.* **118**, 247601 (2017).
- [20] J. Zhang, X. Tan, M. Liu, S. W. Teitelbaum, K. W. Post, F. Jin, K. A. Nelson, D. N. Basov, W. Wu, and R. D. Averitt, *Nat. Mater.* **15**, 956 (2016).
- [21] T. Li, A. Patz, L. Mouchliadis, J. Yan, T. A. Lograsso, I. E. Perakis, and J. Wang, *Nature* **496**, 69 (2013).
- [22] D. M. Pajerowski, D. K. Pratt, S. E. Hahn, W. Tian, G. E. Granroth, A. I. Kolesnikov, A. A. Taskin, Y. Ando, and R. J. McQueeney, *Phys. Rev. B* **101**, 064418 (2020).
- [23] S. Shapiro, M. Iizumi, and G. Shirane, *Phys. Rev. B* **14**, 200 (1976).
- [24] S. Borroni, J. Teyssier, P. Piekarczyk, A. B. Kuzmenko, A. M. Oles, J. Lorenzana, and F. Carbone, *Phys. Rev. B* **98**, 184301 (2018).
- [25] Y. Tomioka, A. Asamitsu, H. Kuwahara, Y. Moritomo, and Y. Tokura, *Phys. Rev. B* **53**, R1689(R) (1996).
- [26] S. Nair and A. Banerjee, *J. Phys.: Condens. Matter* **16**, 8335 (2004); *Phys. Rev. Lett.* **93**, 117204 (2004).
- [27] S. Dash, Kranti Kumar, A. Banerjee, and P. Chaddah, *Phys. Rev. B* **82**, 172412 (2010).
- [28] See Supplemental Material at <http://link.aps.org/supplemental/10.1103/PhysRevB.102.201109> for Fig. S1.
- [29] S. Merten, O. Shapoval, B. Damaschke, K. Samwer, and V. Moshnyaga, *Sci. Rep.* **9**, 2387 (2019).
- [30] P. Postorino, A. Congeduti, P. Dore, A. Sacchetti, F. Gorelli, L. Ulivi, A. Kumar, and D. D. Sarma, *Phys. Rev. Lett.* **91**, 175501 (2003).
- [31] I. Loa, P. Adler, A. Grzechnik, K. Syassen, U. Schwarz, M. Hanfland, G. K. Rozenberg, P. Gorodetsky, and M. P. Pasternak, *Phys. Rev. Lett.* **87**, 125501 (2001).
- [32] A. K. Parmanik and A. Banerjee, *Phys. Rev. B* **79**, 214426 (2009).
- [33] J. Lee, E. Granato, and J. M. Kosterlitz, *Phys. Rev. B* **44**, 4819 (1991).
- [34] M. Tissier, B. Delamotte, and D. Mouhanna, *Phys. Rev. B* **67**, 134422 (2003).
- [35] J. Lin, P. Tong, D. Cui, C. Yang, J. Yang, S. Lin, B. Wang, W. Tong, L. Zhang, Y. Zou, and Y. Sun, *Sci. Rep.* **5**, 7933 (2014).
- [36] Sh. B. Abdulvagidov, Sh. Z. Djabrailov, B. Sh. Abdulvagidov, and A. I. Kurbakov, *J. Exp. Theor. Phys.* **130**, 528 (2020).
- [37] R. M. Fernandes, A. E. Bohmer, C. Meingast, and J. Schmalian, *Phys. Rev. Lett.* **111**, 137001 (2013).
- [38] P. Massat, Y. Quan, R. Grasset, M.-A. Measson, M. Cazayous, A. Sacuto, S. Karlsson, P. Strobel, P. Toulemonde, Z. Yin, and Y. Gallais, *Phys. Rev. Lett.* **121**, 077001 (2018).
- [39] S. Miyasaka, T. Okuda, and Y. Tokura, *Phys. Rev. Lett.* **85**, 5388 (2000).